Generation of Runaway Electrons during the Thermal Quench in Tokamaks

P. Aleynikov[1] and B. N. Breizman[2]

[1]*Max-Planck-Institut für Plasmaphysik, Garching, Germany*
[2]*University of Texas at Austin, Austin, TX 78712, USA*
Corresponding Author: P. Aleynikov, pavel.aleynikov@ipp.mpg.de

A consistent description of runaway electron (RE) generation in plasma disruptions remains an open physics issue. The possibility of the formation of high postdisruption RE currents raises safety-related concerns for large tokamaks, such as ITER. Although the avalanche mechanism of RE production is anticipated to be the dominant mechanism in ITER [1], the avalanche multiplication of the runaways after the thermal quench still requires a seed RE current. The need for reliable prediction of the RE generation in ITER calls for additional attention to the primary (seed) population of the RE.

We present an advanced description of electron kinetics during impurity-dominated thermal quenches in tokamaks. A 2D Fokker–Planck equation for the hot electrons and a power balance equation for the bulk plasma are solved self-consistently, with impurity radiation as the dominant energy loss mechanism. The post-thermal-quench (but pre-current-quench) RE density, energy and current are found for a broad range of initial plasma parameters (density, current density, temperature and impurity concentration), including those of interest for ITER.

We find that runaway formation is less efficient in plasmas with high pre-quench temperatures. In particular, we do not expect any significant runaway seed in a 10 keV plasma with a density of $10^{20}/\mathrm{m}^3$ when the amount of injected argon is less than $5 \times 10^{19}/\mathrm{m}^3$, while in a 2 keV plasma of the same density a significant RE population forms if $2 \times 10^{19}/\mathrm{m}^3$ of argon is injected. We also find that runaway production increases for heavier injection of impurities up to prompt conversion of the total pre-quench current into the runaway current in the case of abundant impurities. The mean kinetic energy of RE population is in this case limited to rather moderate values (sub-MeV), asymptotically approaching those of the near-threshold regime [2].

We finally conclude that the nonuniformity of the plasma creates a possibility for the post-quench current to be carried by two distinct runaway populations (a sub-MeV and an ultrarelativistic).

References

[1] M. N. Rosenbluth and S. V. Putvinski, Nucl. Fusion **37**, 1355 (1997).
[2] P. Aleynikov and B. N. Breizman, Phys. Rev. Lett. **114**, 155001 (2015).

Work supported by ITER Contract No. ITER/CT/15/4300001178 and U.S. Department of Energy Contract No. DE-FG02-04ER54742.

Published as a journal article in Nuclear Fusion
http://iopscience.iop.org/article/10.1088/1741-4326/aa5895

Generation of Runaway Electrons During the Thermal Quench in Tokamaks

Pavel Aleynikov[1] and Boris N. Breizman[2]

[1]Max-Planck-Institut für Plasmaphysik, Greifswald, German
[2]Institute for Fusion Studies, The University of Texas, Austin, TX 78712, USA

Corresponding Author: pavel.aleynikov@ipp.mpg.de

Abstract:
A consistent description of runaway electron (RE) generation in plasma disruptions remains an open physics issue. The possibility of the formation of high post-disruption RE currents raises safety-related concerns for large tokamaks, such as ITER. Although the avalanche mechanism of RE production is anticipated to be the dominant mechanism in ITER, the avalanche multiplication of the runaways after the thermal quench still requires a seed RE current. The need for reliable prediction of the RE generation in ITER calls for additional attention to the primary (seed) population of the RE. We present a systematic description of electron kinetics during impurity dominated thermal quenches. We demonstrate that prompt conversion of the total pre-quench current into the sub-MeV RE current is feasible in the case of abundant impurity injection. The subsequent decay of such RE current should be governed by the "near-threshold regime" and prescribed by the impurity amount. We find that the runaway seed density is a non-monotonic function of the pre-quench plasma temperature and that the seed current tends to be restrictively small in plasmas with high pre-quench temperatures, which is likely to cause non-monotonic seed RE profiles in ITER and future high-temperature tokamaks. The non-uniformity of the plasma creates a possibility for the post-quench current to be carried by two distinct runaway populations (a sub-MeV and an ultra-relativistic).

Runaway electron (RE) generation in plasma disruptions remains an open physics issue for large tokamaks, such as ITER. Although the avalanche mechanism of RE production is anticipated to be the dominant mechanism in ITER [1], the avalanche multiplication of the runaways still requires a seed RE current. The need for reliable model for the RE in ITER calls for additional attention to the primary (seed) RE population.

Two main mechanisms were recognised in the past as the RE seed providers: (a) the diffusive leak of electrons from the maxwellian core into the high-energy "runaway" region under the influence of the driving electric field [2, 3, 4] ("Dreicer generation"), and (b) survival of the "hot-tail" during thermal quench (TQ) [5, 6, 7].

The hot tail mechanism was proposed in Refs. [5, 6] and studied subsequently in Refs. [8, 9, 10, 11]. Its analytical study in Refs [8, 9] is limited to the case when the cooling rate is much lower than the collision frequency, which does not apply to the mitigated TQ. Refs. [10, 11] extend the analysis to the case of fast (exponential) cooling and to a self-consistent calculation of the plasma temperature, respectively. However,

they involve an oversimplified 1D kinetic equation for electrons that does not include the driving electric field, underestimating the seed current.

This paper presents a recently developed description of electron kinetics during impurity dominated TQ [12].

The amount of injected impurities will govern the resulting evolution of the electron distribution function. The situation depends on how the rate of impurity ionization is related to the heating rate of the cold electrons released via ionization. In the extreme case of very dilute impurities the cold electron production rate is much lower than their heating rate, so that the new electrons mix quickly with the hot population. In the opposite limit of heavy injection, the released electrons form a cold maxwellian population via their mutual collisions, because their collision frequency is much greater than that of the hot population. This naturally creates a two-component electron distribution.

The impurity densities of interest for mitigated disruptions tend to be in the range that results in a two-component electron distribution. Consequently, we herein consider a hot population with an initial density $n^0_{\rm hot}$ and a cold population $n_{\rm cold}$ that forms via ionization of the injected impurities and partly via slowing down of the hot electrons into the cold core.

The two-component electron distribution suggests the following energy balance scenario. The hot electrons loose their energy via Coulomb collisions with the cold electrons. The energy loss mechanism for the cold electrons is assumed to be line radiation. We neglect excitation of impurities by the hot electrons, because the cold electron density quickly raises above $n_{\rm hot}$ and because the line excitation rate decreases with the incident electron energy. The maxwellian cold population is in the "coronal-type" equilibrium. We assume the impurity density to be spatially uniform. This implies that the hot electron mean-free path is greater than the machine radius, so that the rate of hot electron cooling is determined by the average value of cold electron density. It should however be noted that equilibration of the impurities within the magnetic surface may require a substantial time in the case of localized injection (as seen, for example, from NIMROD simulations [13]). If the impurity density remains localized, then our uniform density assumption actually underestimates the radiated power and thereby the electron cooling down rate. We note that spatial non-uniformity enhances line radiation. Also, an expansion of the impurity cloud along the magnetic field can accelerate electron cooling due to electron energy transfer to the ions.

We neglect collisions between the hot electrons and consider only their collisions with the cold background. We also neglect the avalanche multiplication of electrons via knock-on collisions, because of the shortness of the TQ. These assumptions simplify the collisional integral for the hot electrons, so that the distribution function F of the hot electrons satisfies the following Fokker-Planck equation [4, 1]:

$$\begin{aligned}&\frac{\partial F}{\partial s}+\frac{\partial}{\partial p}\left[E\cos\theta-1-\frac{1}{p^2}\right]F=\\&\frac{1}{\sin\theta}\frac{\partial}{\partial\theta}\sin\theta\left[E\frac{\sin\theta}{p}F+\frac{(Z_{eff}+1)}{2}\frac{\sqrt{p^2+1}}{p^3}\frac{\partial F}{\partial\theta}\right],\end{aligned}\tag{1}$$

where p is the particle momentum (normalized to mc), θ is the pitch-angle, s is the dimensionless time variable defined as $\frac{ds}{dt} = \frac{1}{\tau} \equiv \frac{e^4 n_{\rm cold} \Lambda}{4\pi\varepsilon_0^2 m_0^2 c^3}$, E is the ratio of the inductive electric field to the instantaneous critical field $E_c \equiv \frac{m_0 c}{e}\frac{1}{\tau}$, and $Z_{\rm eff}$ is the effective ion charge. The instantaneous density of the hot electrons is given by $n_{\rm hot} = \int F dp \sin\theta d\theta$. Note that $n_{\rm cold}$, τ, $Z_{\rm eff}$, and $n_{\rm hot}$ are generally time-dependent quantities, and that $n_{\rm hot}$ can decrease significantly over time as the hot electrons slow down into the bulk.

The mean kinetic energy of the hot population is relatively low during the TQ, in which case $Z_{\rm eff}$ is the average impurity charge state. However, the meaning of $Z_{\rm eff}$ needs to be refined to model the subsequent current quench process (see [14]).

The cold electrons are characterized by their conductivity $\sigma_{\rm cold}$, which we first treat as a given. We then include their energy balance into consideration and treat $\sigma_{\rm cold}$ self-consistently as the Spitzer conductivity of the maxwellian core. The magnetic energy cannot change significantly during the TQ, because the system of interest is highly inductive. We therefore assume conservation of the current density to calculate the electric field E, i.e we combine Eq. (1) with

$$j_0 = \int e v_\parallel F dp \sin\theta d\theta + \sigma_{\rm cold} E E_c, \tag{2}$$

where j_0 is the pre-quench plasma current density and $v_\parallel$ is the parallel component of the electron velocity.

The initial distribution function of the hot electrons is chosen to be Maxwellian ($F_{\rm M}$) with $n_{\rm hot}^0$, pre-quench temperature T_0, and with a small correction ($\delta F = -E\cos\theta \frac{p^2}{Z_{\rm eff}} \frac{\partial F_{\rm M}}{\partial p}$) that provides Spitzer conductivity.

A complete model must include self-consistent calculation of the cold plasma temperature. We herein assume that the dominant energy loss channel for the cold plasma is radiation. The cold electron density $n_{\rm cold}$ is then given by

$$n_{\rm cold} = (n_{\rm hot}^0 - n_{\rm hot} + n_{\rm imp} Z_{\rm imp}(T)), \tag{3}$$

where $Z_{\rm imp}$ is the average charge state of the impurity, as calculated in Ref. [16]. The power balance equation for the cold electrons is

$$\frac{\partial (W_{th} + W_i(T))}{\partial t} = P_s(F) + \frac{j_c^2}{\sigma_{\rm cold}} - n_{\rm imp} n_{\rm cold} L(T), \tag{4}$$

where $W_{th} = \frac{3}{2} n_{\rm cold} T$ is the kinetic energy density of the cold population, W_i is the ionization energy, P_s is the stopping power released by the hot population via Coulomb collisions, and $L(T)$ is the radiative cooling coefficient [16]. The ionization energy is approximately represented by the sum of the ionization energies for the atomic levels up to $Z_{\rm imp}(T)$. The values of the effective ion charge $Z_{\rm eff}$ in Eq. (1) and the expression for $\sigma_{\rm cold}$ also change with time and temperature according to the definition of $Z_{\rm eff} = (n_{\rm hot}^0 - n_{\rm hot} + n_{\rm imp} Z_{\rm imp}^2(T))/n_{\rm cold}$.

In the limit of very low conductivity of the bulk ($\sigma_{\rm cold} = 0$) all the current has to be carried by the hot population. Figure 1 shows the evolving distribution function F and

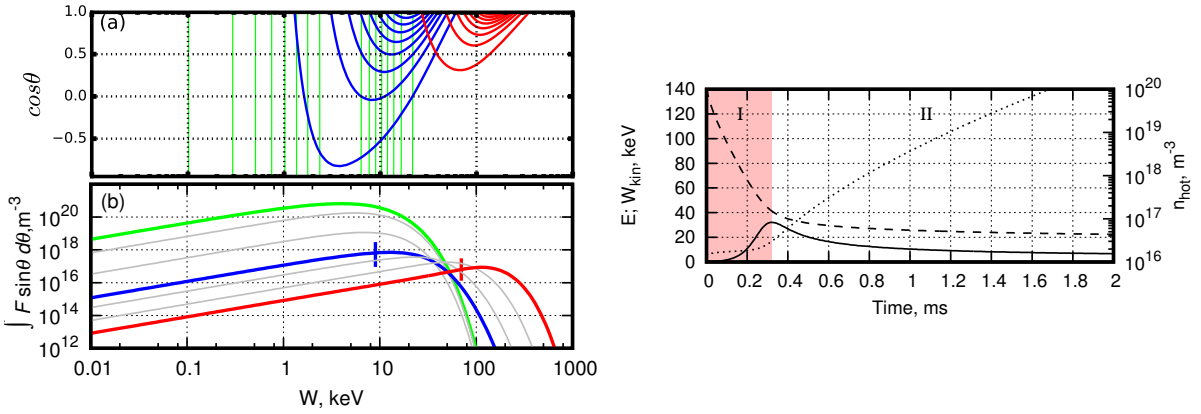

FIG. 1: On the left: Snapshots of the evolving (a) momentum space distribution function F and (b) its isotropic part $\int F \sin\theta d\theta$ at 0 ms *(green),* 0.3 ms *(blue) and* 1.5 ms *(red). The contours in the 2D plot (a) mark 0.9, 0.8 ... 0.2 of the F maximum value. The red and blue vertical strokes mark the entrance energies to the runaway regime. On the right: Hot population density $n_{\rm hot}$ (dashed), electric field E (solid) and mean kinetic energy $W_{\rm kin}$ (dotted).*

its isotropic part $\int F \sin\theta d\theta$ for such a case. The input parameters in this calculation are: $T_0 = 4$keV, $n^0_{\rm hot} = 10^{20}{\rm m}^{-3}$, $Z_{\rm eff} = 2.0$, and $j_0 = 1{\rm MA/m}^2$.

As seen in Fig. 1, the nearly isotropic initial distribution (green contours) transforms into a beam-like distribution (red contours). This transformation has two phases. Phase I (pink color in Fig. 1) is characterised by a very steep rise of the electric field and a significant drop of the hot electron density $n_{\rm hot}$. The mean electron energy does not change much during this phase. The electric field rises until the hot electrons reach an order-of-unity anisotropy and thereby enter the runaway regime (phase II). During phase II the friction force is unable to balance the electric field drive for the current-carrying electrons. As a result, their energy increases whereas the decay of their density ceases as these electrons form a beam-like distribution and approach relativistic energies (blue and red contours in Fig. 1). The electric field decays in step with their acceleration, and it eventually approaches the critical level over a long time.

Equations (1), (2), (3) and (4) form a closed set that describes the hot and the cold populations self-consistently. We solve these equations numerically. Their solutions for $n^0_{\rm hot} = 10^{20}{\rm m}^{-3}$, $T_0 = 4$keV, $j_0 = 1{\rm MA/m}^2$, and various densities of the injected argon impurity are shown in Fig. 2. At first, the hot population quickly deposits most of its energy to the cold plasma. Some of this energy is immediately lost on ionization, and the rest dissipates via line-radiation on a longer timescale. Heavy injection of impurities does not allow the cold electron temperature to grow significantly. In this case the hot population evolves similarly to the zero-conductivity case that renders prompt conversion of the total current into the runaway current.

At lower densities of impurities, the temperature rises to a level at which the cold plasma can carry a significant fraction of the total current, enabling a nearly unimpaired slowing down of the hot population (red curves in Fig. 2). In the Cyan, Purple, Blue

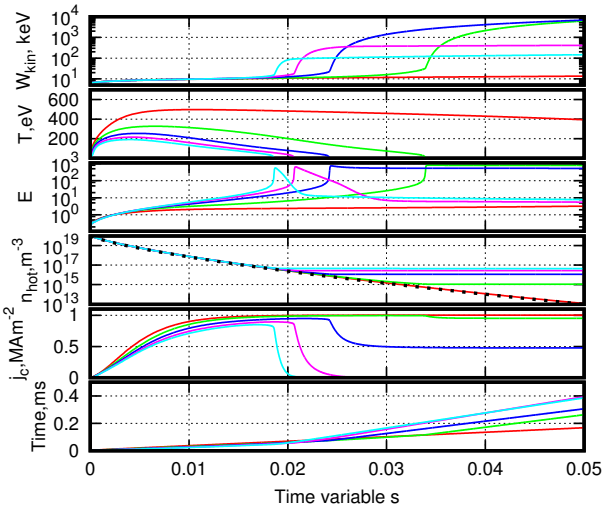

FIG. 2: Top to bottom: Mean kinetic energy of the hot population ($W_{\rm kin}$), cold plasma temperature (T), electric field (E), hot population density ($n_{\rm hot}$), cold plasma current (j_c), and real time. The colors mark argon content in units of $10^{20}m^{-3}$: Cyan - 0.7, Purple - 0.6, Blue - 0.5, Green - 0.4, - Red 0.3.

and Green cases in Fig. 2, the decay of the hot population stops when the cold plasma temperature drops to its minimal value. In what follows, we label the corresponding value of s as s_0 (the "TQ duration"). The electric field reaches its maximum at this point. If the density of the surviving hot electrons is sufficient to carry the total current (Cyan and Purple cases), then the subsequent evolution is a decay of the electric field with a moderate acceleration of the hot population (phase II of the $\sigma_{\rm cold} = 0$ case, i.e. prompt conversion case). The resulting mean energy of the hot population is in a sub-MeV range.

If the density of the surviving hot electrons is too low to carry the full current at s_0 (Green and Blue cases), then a fraction of the current is carried by the cold ohmic plasma. In this case, the long-lasting strong electric field accelerates the surviving hot population to ultra-relativistic energies until new factors (presumably synchrotron radiation) limit the energy gain [17].

Figure 3a presents a contour plot of the ultimate density of the hot population $n_{\rm hot}^{\infty}$ normalized to j_0/ec (solid contours) together with the mean kinetic energy $W_{\rm kin}$ (color-coded) for $n_{\rm hot}^0 = 10^{20}{\rm m}^{-3}$ and $j_0 = 1{\rm MA/m}^2$.

In contrast with Ref.[6], we find that the density of the surviving hot population grows with $n_{\rm imp}$ for any initial plasma temperature until full conversion of the current into the RE current. The mean energy of the hot population is in a sub-MeV range in the full conversion regime (the area to the right of 1.0 contour in Fig. 3), whereas incomplete conversion can entail much higher energies. We also note that $n_{\rm hot}^{\infty}$ is a non-monotonic function of T_0 for a given amount of impurities. This is clarified in Fig. 4, where the cold plasma temperature and the hot population density evolution are plotted for $n_{\rm hot}^0 = 10^{20}{\rm m}^{-3}$, $j_0 = 1{\rm MA/m}^2$, $n_{\rm Ar} = 0.6 \cdot 10^{20}{\rm m}^{-3}$ and a number of pre-quench

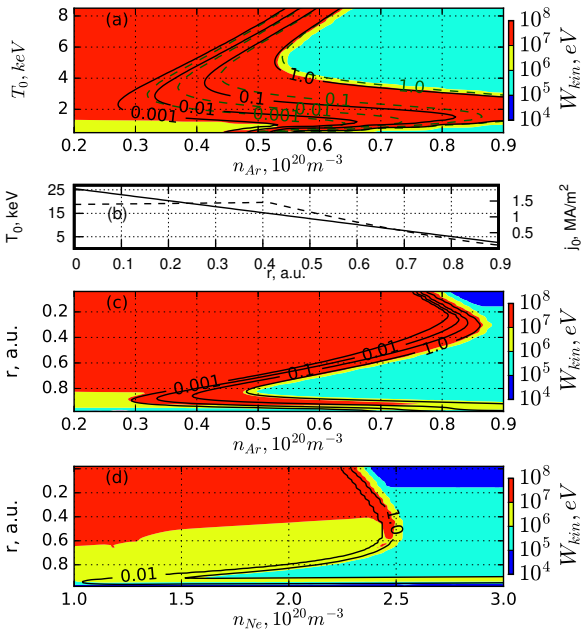

FIG. 3: Contour plots of the surviving hot population, $n^{\infty}_{\rm hot}$, normalized to j_0/ec (solid contours), for a range of initial electron temperatures T_0 and injected impurity densities. Color-coded is the mean kinetic energy of the hot population ($W_{\rm kin}$). Panel (a) shows $n^{\infty}_{\rm hot}$ for $j_0 = 1{\rm MA/m}^2$. Panels (c) and (d) show radial dependencies of $n^{\infty}_{\rm hot}$ for argon and neon, respectively, when j_0 (dashed curve in plot (b)) is linked to T_0 (solid curve in plot (b)).

plasma temperatures. We observe that the TQ-length (s_0) increases monotonically with the growth of initial temperature, while the hot population decay rate decreases. As a result, the surviving hot population density (read from the horizontal part of the density curves) is the highest for the Blue case in Fig. 4.

The pre-quench radial profile of the plasma current is typically non-uniform in tokamaks. As a result, the density of the runaway seed can also vary significantly over the plasma cross section [18]. In order to study the radial distribution of the seed current, we have performed calculations in which the initial current density j_0 is linked to the initial temperature T_0, as shown in Fig. 3b. This figure approximates the profiles expected in the 15MA ITER scenario (Fig. 4 from [19]). Figures 3c and 3d show the results of these calculations for argon and neon ($n^0_{\rm hot} = 10^{20}{\rm m}^{-3}$). These gases are the main candidates for the ITER disruption mitigation system [20, 15]. In contrast with Ref. [18], which relies on the Dreicer mechanism of the RE seed production, we find that the seed profile is not peaked in the plasma core. In particular, for a radially flat argon density of $0.5 \cdot 10^{20}{\rm m}^{-3}$, the seed REs will occupy a radial area corresponding to $T_0 = 1 - 7$keV. Prompt conversion of the local current density into a sub-MeV RE current is expected near 4keV, while ultra-relativistic REs in the 6keV area are merely a seed for subsequent avalanche development. We thus note that the non-uniformity of the plasma creates a possibility

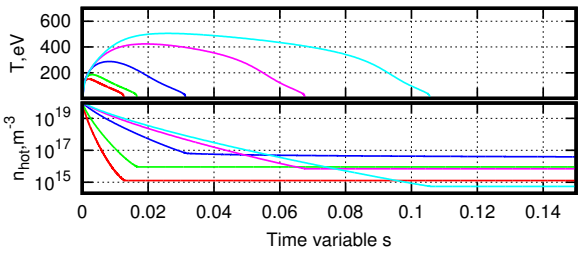

FIG. 4: Cold plasma temperature (T) (top) and hot population density ($n_{\rm hot}$) (bottom) evolution. The colors mark different pre-quench plasma temperature: Cyan - 9keV*, Purple* - 8keV*, Blue* - 6keV*, Green* - 3keV*, Red* - 2keV*.*

for the post-quench current to be carried by two distinct runaway populations (a sub-MeV and an ultra-relativistic), and that the seed RE profile is not necessarily peaked at the plasma core. It is also essential that the electric field drops only to $E \approx 4-8$ in the prompt conversion region in our calculations, because it takes a much longer time to asymptotically approach the near-threshold regime [17]. The simultaneous presence of ultra-relativistic REs and a significant sub-MeV RE population in an elevated electric field is in line with experimental observations [21].

In summary: 1) We conclude that prompt conversion of the total pre-quench current into the sub-MeV RE current is feasible in the case of abundant impurity injection. An attractive feature of this regime is that the resulting rate of the current decay after the TQ is sufficiently low to envisage plasma position control in disruption. The current decay should follow the near-threshold scenario [17, 23] governed by the amount of impurity. 2) Our calculations quantify limitations on impurity injection for runaway-free disruptions, assuming that the dominant energy loss channel for the cold plasma is radiation. The upper limits for ITER-relevant conditions are $3\cdot10^{19}\mathrm{m}^{-3}$ for argon and $10^{20}\mathrm{m}^{-3}$ for neon. A significant runaway population at lower densities should be viewed as an evidence of anomalous electron heat losses. 3) We find that the runaway seed density is a non-monotonic function of the pre-quench plasma temperature, which is likely to cause non-monotonic seed RE profiles in ITER and future high-temperature tokamaks, in contrast with the modern lower temperatures experiments. This calls for additional attention to MHD stability of the post-quench plasmas. 4) We find that the non-uniformity of the plasma creates a possibility for the post-quench current to be carried by two distinct runaway populations (a sub-MeV and an ultra-relativistic).

The authors appreciate helpful discussions with P. Helander, S. Konovalov, M. Lehnen and H. Smith. Work supported by ITER Contract No. ITER/CT/15/4300001178 and the U.S. Department of Energy Contract No. DEFG02-04ER54742.

References

[1] ROSENBLUTH M.N., PUTVINSKI S.V., Nucl. Fusion **37** (1997) 1355

[2] DREICER H., Phys. Rev. **115** (1959) 238; **117** (1960) 239

[3] GUREVICH A.V., Sov. Phys. JETP **12** (1961) 904

[4] CONNOR J.W., HASTIE R.J., Nucl. Fusion **15** (1975) 415

[5] CHIU S.C., ROSENBLUTH M.N., HARVEY R.W., CHAN V.S., Nucl. Fusion **38** (1998) 1711

[6] HARVEY R.W., CHAN V.S., CHIU S.C., EVANS T.E., ROSENBLUTH M.N., WHYTE D.G., Phys. Plasmas **7** (2000) 4590

[7] MARTIN-SOLIS J.R., ESPOSITO B., SANCHEZ R., POLI F.M., PANACCIONE L., PRL **97** (2006) 165002

[8] HELANDER P., SMITH H., FULOP T., ERIKSSON L.-G., Phys. Plasmas **11** (2004) 570

[9] SMITH H., HELANDER P., ERIKSSON L.-G., FULOP T., Phys. Plasmas **12** (2005) 12250

[10] SMITH H.M., VERWICHTE E., Phys. Plasmas **15** (2008) 072502

[11] FEHER T., SMITH H.M., FULOP T., GAL K., PPCF **53** (2011) 035014

[12] ALEYNIKOV P., BREIZMAN B.N., *Generation of runaway electrons during the thermal quench in tokamaks*, submitted for publication, Nucl. Fusion (2016)

[13] IZZO V.A., et al. Nucl. Fusion **55** (2015) 073032

[14] ALEYNIKOV P., et. al *in Proceedings of the 25th IAEA Fusion Energy Conference, St. Petersburg, Russian Federation, 2014,* pp. TH/P3-38.

[15] HOLLMANN E., et al. Phys. Plasmas **22** (2015) 021802

[16] SUMMERS H.P., et al., Plasma Phys. Control. Fusion **48**, (2006) 263-293 http://www.adas-fusion.eu/

[17] ALEYNIKOV P., BREIZMAN B.N., PRL **114** (2015) 155001

[18] ERIKSSON L.-G., HELANDER P., ANDERSSON F., ANDERSON D., LISAK M., PRL **92** (2004) 205004

[19] GREEN B.J., Plasma Phys. Control. Fusion **45** (2003) 687

[20] LEHNEN M., et al. J. Nucl. Mater **463** (2015) 39

[21] HOLLMANN E., et al. Phys. Plasmas **22** (2015) 056108

[22] LEHNEN M., et al. J. Nucl. Mater. **390-391** (2009) 740

[23] BREIZMAN B.N., Nucl. Fusion **54** (2014) 072002